Carbonation of Limestone Derived CaO for Thermochemical Energy Storage: From Kinetics to Process Integration in Concentrating Solar Plants

C. Ortiz,[*,†] J. M. Valverde,[†] R. Chacartegui,[‡] and L. A. Perez-Maqueda[§]

[†]Facultad de Física, Universidad de Sevilla, Avenida Reina Mercedes s/n, 41012 Sevilla, Spain

[‡]Escuela Técnica Superior de Ingeniería, Universidad de Sevilla, Camino de los descubrimientos s/n, 41092 Sevilla, Spain

[§]Instituto de Ciencia de Materiales de Sevilla (C.S.I.C.-Univ. Sevilla), Américo Vespucio 49, 41092 Sevilla, Spain

ABSTRACT: Thermochemical energy storage (TCES) is considered as a promising technology to accomplish high energy storage efficiency in concentrating solar power (CSP) plants. Among the various possibilities, the calcium-looping (CaL) process, based on the reversible calcination−carbonation of $CaCO_3$ stands as a main candidate due to the high energy density achievable and the extremely low price, nontoxicity, and wide availability of natural CaO precursors such as limestone. The CaL process is already widely studied for CO_2 capture in fossil fuel power plants or to enhance H_2 production from methane reforming. Either one of these applications requires particular reaction conditions to which the sorbent performance (reaction kinetics and multicycle conversion) is extremely sensitive. Therefore, specific models based on the conditions of any particular application are needed. To get a grip on the optimum conditions for the carbonation of limestone derived CaO in the CaL-CSP integration, in the present work is pursued a multidisciplinary approach that combines theoretical modeling on reaction kinetics, lab-scale experimental tests at relevant CaL conditions for TCES, process modeling, and simulations. A new analytic equation to estimate the carbonation reaction rate as a function of CO_2 partial pressure and temperature is proposed and validated with experimental data. Using the kinetics analysis, a carbonator model is proposed to assess the average carbonation degree of the solids. After that, the carbonator model is incorporated into an overall process integration scheme to address the optimum operation conditions from thermodynamic and kinetics considerations. Results from process simulations show that the highest efficiencies for the CaL-CSP integration are achieved at carbonator absolute pressures of ∼3.5−4 bar, which leads to an overall plant efficiency (net electric power to net solar thermal power) around 41% when carbonation is carried out at 950 °C under pure CO_2.

KEYWORDS: Calcium looping, Carbonation kinetics, CSP, Energy storage, Limestone
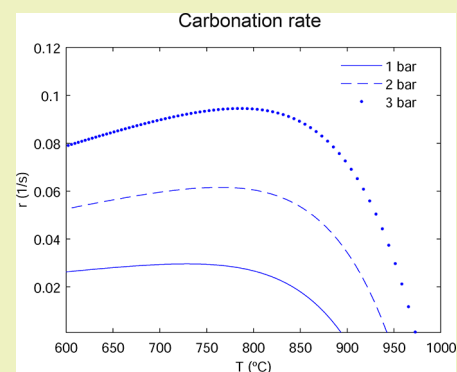
INTRODUCTION

The main challenge to increase the share of renewable energy in the global energy mix is dispatchability. Regarding this issue, concentrating solar power (CSP) shows several advantages over solar photovoltaic (PV) and wind due to the relatively low cost and feasible integration of thermal energy storage technologies in large-scale facilities compared to battery storage.[1−3] Thus, thermal energy storage (TES) in CSP plants has gained attention in the last years as demonstrated by the current data on commercial CSP facilities. A 42% of commercial CSP plants in operation incorporate TES systems while this percentage rises up to 83% for those planned and under development.[4]

Most commercial TES systems are based on sensible heat storage by means of molten salts, which allows plant operation for up to 15 h in the absence of direct solar irradiation. However, molten salt based systems have several drawbacks that penalize the performance of CSP plants. On one hand, the maximum working temperature is limited to ∼560 °C to avoid

salt degradation, which reduces the power cycle efficiency.[5] On the other, there is a minimum working temperature of ∼200 °C to avoid salt solidification,[6] which demands a significant amount of energy to keep the molten salts from solidifying when the plant is out of operation. Thus, annual efficiencies for CSP plants with tower technology are currently found in the range 14−18%[7] with a power cycle efficiency usually lower than 38%.[4] Salt corrosiveness is also a serious issue that requires the use of expensive highly resistant materials for transport and storage.[8,9]

Thermochemical energy storage (TCES) is a promising alternative to TES to overcome these drawbacks in addition to providing other advantages such as the possibility to store energy in the long term and a relatively higher energy density.[10,11] Among the diverse TCES systems proposed, the $CaCO_3$/CaO

system based on the cyclic calcination/carbonation of $CaCO_3$ (calcium-looping)

$$CaCO_{3(s)} \rightleftarrows CaO_{(s)} + CO_{2(g)} \quad \Delta H_r^0 = 178 \, \frac{kJ}{mol} \quad (1)$$
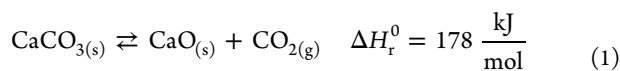
stands as a promising alternative for its high energy density and the extremely low price, nontoxicity, and wide availability of natural CaO precursors such as limestone or dolomite.[12] Thus, the calcium-looping (CaL) process shows a theoretical energy density around 3−4 GJ/m^3[13−16] depending on storage temperatures and pressure and the multicycle performance of the Ca-based materials employed. In the case of commercial CSP plants with tower technology based on a two tank molten salts system, the energy density is just around 0.4 GJ/m^3.[17]

The CaL process is initiated by $CaCO_3$ decomposition in the calciner to produce CaO and CO_2, which are stored separately. When energy is needed, CaO and CO_2 are brought together in a separate reactor to release the stored energy by means of the exothermic carbonation reaction. Before being considered as a potential TCES system in the late 1970s,[18−20] the use of CaO-based materials was already used for CO_2 capture to enhance H_2 production from methane reforming as early as 1933.[21] More recently, the CaL process has been widely studied for postcombustion CO_2 capture (PCC) in fossil power plants where it has been successfully demonstrated at the 1−2 MWth pilot scale.[22−26]

Importantly, the optimum conditions to carry out the CaL process depend on the particular application. They may vary notably from one case to another, which affects critically the CaO multicycle performance.[27] Thus, process conditions for postcombustion CO_2 capture involve decomposition of $CaCO_3$ at high temperature (around 950 °C) under high CO_2 partial pressure and carbonation at ~650 °C under low CO_2 partial pressure (~0.15 bar).[28−30] On the other hand, CaL conditions to achieve high overall efficiency for TCES and electricity generation in CSP plants are radically different.[31] In this application, carbonation would be carried out at high CO_2 partial pressure and high temperature (around or above 850 °C) whereas calcination could be performed at relatively low temperature (~700 °C) using a gas easily separable from CO_2 under which the reaction kinetics is enhanced such as superheated steam or helium.[32−34] The diverse CaL conditions used for PCC and TCES lead also to different multicycle CaO performances[35,36] and reaction kinetics behavior.[33,37] In this regard, there are a wide number of carbonation kinetics studies focused on CO_2 capture conditions,[38−40] but those considering the specific conditions for TCES application are scarce.[41]

This manuscript presents a novel carbonation kinetics model focused on the conditions that lead to an efficient energy integration of CSP-CaL plants for TCES. A new analytic expression is proposed to estimate the carbonation reaction rate as a function of temperature and pressure. The new reaction kinetics expression shows a good agreement with experimental data and previous works.[41] Using the equation derived from this study together with thermogravimetric analysis results on the multicycle CaO conversion at relevant CaL conditions for TCES, a carbonator model is developed to analyze the carbonation behavior after a long number of cycles in the industrial process. Next, a CSP-CaL plant has been modeled to analyze the overall efficiency of the plant (defined as the ratio between net electric power production and net solar thermal power entering the calciner) and to envisage the conditions that maximize energy efficiency. Thus, our multidisciplinary approach combines reaction kinetics theory and lab-scale tests at relevant CaL

conditions with process modeling and simulations in order to further explore the optimum process conditions for the integration of the CaL process into CSP plants.

The manuscript is structured as follows: A first section on carbonation kinetics describes in detail the kinetics model developed starting from the analysis of carbonation mechanism. Thermogravimetric analysis (TGA) experimental results on the carbonation kinetics are also presented and compared with theoretical predictions. The next section develops a carbonator model, which is built upon TGA and kinetics theory developed in previous sections. Later on, a section focused on the CSP-CaL integration describes a conceptual engineering process to incorporate TCES into CSP plants.
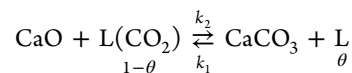
■ CARBONATION KINETICS

Let us consider an ideally flat surface of a CaO solid where carbonation proceeds in a gas environment at a given temperature and CO_2 partial pressure P. Arguably, the overall carbonation mechanism consists of two stages as usually observed in heterogeneous gas/solid reactions.[42] In the first stage, CO_2 molecules become physically adsorbed on the CaO surface after which a chemical reaction stage yields $CaCO_3$:

Stage I CO_2 adsorption

$$CaO + \underset{\theta}{L} + \underset{P}{CO_2} \underset{k_d}{\overset{k_a}{\rightleftarrows}} CaO + \underset{1-\theta}{L(CO_2)}$$
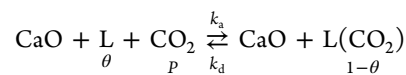
Stage II Chemical reaction

$$CaO + \underset{1-\theta}{L(CO_2)} \underset{k_1}{\overset{k_2}{\rightleftarrows}} CaCO_3 + \underset{\theta}{L}$$

Here L represents the active site wherein physical adsorption of a CO_2 molecule takes place before the chemical reaction occurs, k_i are the reaction rate constants, θ is the fraction of active empty sites, and $1 - \theta$ is the fraction of active sites filled with adsorbed CO_2 molecules.

According to the pseudosteady state hypothesis,[43] the rate of increase of the fraction of active sites filled with CO_2 by adsorption must balance the rate of decrease of filled active sites by chemical reaction in order not to have a net accumulation of reactive intermediates. Thus, the rates of adsorption r_a and chemical reaction r_2:

$$r_a = k_a \theta P - k_d (1 - \theta) \quad (2)$$

$$r_2 = k_2 (1 - \theta) - k_1 \theta \quad (3)$$

must balance out ($r_a = r_2$), which yields

$$\theta = \frac{k_2 + k_d}{k_a P + k_d + k_1 + k_2} \quad (4)$$

The microscopic reversibility principle determines that for the overall reaction to reach equilibrium ($\theta = \theta_{eq}$, $P = P_{eq}$), the rate of any process in each elementary step must be equal to the rate of its reverse process ($r_a = r_2 = 0$).[44] The microscopic reversibility principle has been successfully applied to the kinetics description of a number of reversible processes such as the dehydrogenation/hydrogenation of MgH_2.[45] This principle leads to

$$\left.\begin{array}{r} k_a \theta_{eq} P_{eq} = k_d (1 - \theta_{eq}) \\ k_2 (1 - \theta_{eq}) = k_1 \theta_{eq} \end{array}\right\} \rightarrow P_{eq}(atm) = \frac{k_1}{k_2} \frac{k_d}{k_a} \quad (5)$$

Assuming, as in most gas—solid heterogeneous reactions,[42] that the rate-limiting step is the chemical reaction stage (k_1, $k_2 \ll k_a P$, k_d) it is

$$\theta \approx \frac{k_d}{k_a P + k_d}$$

$$r \approx r_2 = k_2(1 - \theta) - k_1 \theta$$

Rearranging, we arrive at

$$r \approx a_2 e^{-E_2/RT} \left(\frac{P}{P_{eq}} - 1 \right) \left(\frac{1}{\frac{P}{P_{eq}} + e^{\Delta S_2^0/R} e^{-\Delta H_2^0/RT}} \right) \tag{6}$$

where E_2 is the carbonation activation energy, a_2 is a preexponential factor, and R the gas constant ($k_2 = a_2 e^{-E_2/RT}$). The Van't Hoff equation[42] has been used for the equilibrium constant $K_2 = k_2/k_1 = e^{-\Delta G_2^0/RT}$ being $\Delta G_2^0 = \Delta H_2^0 - T \Delta S_2^0$ the standard free energy change of carbonation.

By using eq 5, we obtain

$$P_{eq}(\text{atm}) = \frac{1}{K_2 K_a} = e^{-(\Delta S_2^0 + \Delta S_a^0)/R} e^{(\Delta H_2^0 + \Delta H_a^0)/RT} \tag{7}$$

where the Van't Hoff equation has been used for the equilibrium constant $K_a = k_a/k_d = e^{-\Delta G_a^0/RT}$, with $\Delta G_a^0 = \Delta H_a^0 - T \Delta S_a^0$ the standard free energy change of adsorption. On the other hand, from thermochemical data,[46−48] the following is inferred:

$$P_{eq} = A e^{-\alpha/T} \tag{8}$$

where $A = 4.083 \times 10^7$ atm, $\alpha = 20474$ K, which from eq 7 yields $\Delta S_2^0 + \Delta S_a^0 = -146$ J/mol·K and $\Delta H_2^0 + \Delta H_a^0 = -170$ kJ/mol. On the other hand, the sum of the standard enthalpy change of adsorption ΔH_a^0 and carbonation ΔH_2^0 is the standard enthalpy change of the overall reaction: $\Delta H_r^0 = \Delta H_a^0 + \Delta H_2^0 = -178$ kJ/mol as independently determined from the difference between the standard enthalpies of formation of the final product ($CaCO_3(s)$) and initial reactants ($CO_2(g)$ and $CaO(s)$). Likewise, it is $\Delta S_r^0 = \Delta S_a^0 + \Delta S_2^0 = -160$ J/mol·K. As should be expected, these independently determined values are similar to those derived from comparison of eqs 7 and 8.

The standard entropy change of adsorption ΔS_a^0 may be obtained from the difference between the standard entropy of adsorbed CO_2 (S_{ad}^0) and the standard entropy of CO_2 in the gas phase ($S_{gas}^0 = 238$ J/mol·K for CO_2). According to Campbell and Sellers,[49] the standard entropy of adsorbed molecules on single crystal surfaces can be well fitted (up to $S_{gas}^0 \approx 60R$) to the universal law $S_{ad}^0 = 0.7 S_{gas}^0 - 3.3R$. Thus, it is $\Delta S_a^0 = S_{ad}^0 - S_{CO2}^0 \cong -92$ J/mol·K. On the other hand, using $\Delta H_a^0 \cong -20$ kJ/mol as a typical value[50] in eq 7, it is

$$\frac{P}{P_{eq}} + e^{\Delta S_2^0/R} e^{-\Delta H_2^0/RT}$$

$$= e^{\Delta S_2^0/R} e^{-\Delta H_2^0/RT} (1 + P e^{\Delta S_a^0/R} e^{-\Delta H_a^0/RT})$$

$$\approx e^{\Delta S_2^0/R} e^{-\Delta H_2^0/RT} \tag{9}$$

for the typical range of carbonation temperatures and CO_2 partial pressures ($P e^{\Delta S_a^0/R} e^{-\Delta H_a^0/RT} \ll 1$), which leads to (eq 6):

$$r \approx a_2 e^{-\Delta S_2^0/R} e^{-E_1/RT} \left(\frac{P}{P_{eq}} - 1 \right) \tag{10}$$

where it has been used $\Delta H_2^0 = E_2 - E_1$, with E_1 the activation energy for chemical decomposition. Using, as estimated above, $\Delta S_a^0 = -92$ J/mol·K and $\Delta S_r^0 = \Delta S_a^0 + \Delta S_2^0 = -160$ J/mol·K, the standard entropy change of carbonation is $\Delta S_2^0 = -68$ J/mol·K whereas the activation energy for chemical decomposition is similar to the overall reaction enthalpy change as measured experimentally:[51] $E_1 \cong 180$ kJ/mol.

Note that for $\frac{P}{P_{eq}} \gg 1$ and using eq 7:

$$r \approx a_2 e^{\Delta S_a^0/R} e^{(-(E_2 - E_d)/RT)} P \tag{11}$$

where $\Delta H_a^0 = E_a - E_d$, being E_d the activation energy for desorption and the activation energy for adsorption E_a is assumed to be negligible.

■ EXPERIMENTAL RESULTS ON THE CARBONATION KINETICS

In this work, thermogravimetric analysis (TGA) tests have been carried out to analyze experimentally the carbonation reaction kinetics depending on the reaction temperatures under pure CO_2 and high temperature as relevant conditions in the CaL-CSP integration for TCES. Natural limestone of high purity (99.6 wt % $CaCO_3$) was used in the tests, which were carried out by employing two different thermogravimetric analyzers (TA Q600 and Setaram LABSYS evo). In all the tests, a small sample mass (10 mg) was employed to minimize mass/heat transfer undesired effects. The limestone samples were calcined at 750 °C under pure N_2 for 5 min after which the temperature was increased to the target carbonation temperature and pure CO_2 at atmospheric pressure was introduced for carbonation to proceed.

Results for the time evolution of CaO conversion during carbonation at different temperatures are shown in Figure 1. As can be
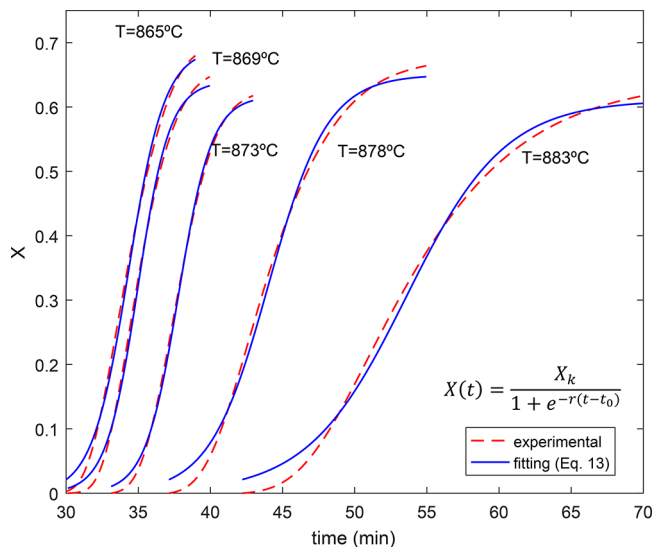

Figure 1. Time evolution of CaO conversion measured experimentally and best fit curves from eq 13. Values of the best fitting parameters (t_0, X_K, and r) are shown in Table 1. Best fitting parameters are plotted in Figure 2 (reaction rate r) and Figure 3 (conversion at the end of the reaction controlled stage X_K).

seen, CaO conversion is hindered as the carbonation temperature approaches the equilibrium temperature ($T \sim 895$ °C under pure CO_2 at atmospheric pressure). As the reaction evolves, the carbonation rate is determined as a function of conversion degree X, and reaction temperature T and pressure P (eq 12). Note that the conversion degree X, which is usually employed to note the conversion of CaO during carbonation, is equivalent to the term α usually employed in kinetics studies.

Table 1. Best Fitting Parameters of Equation 13 to Experimental Data on CaO Conversion for Carbonation under CO_2 at Atmospheric Pressure and Several Carbonation Temperatures

$X(t) = \dfrac{X_k}{1 + e^{-r(t-t_0)}}$	carbonation temperature				
	$T = 865\ °C$	$T = 869\ °C$	$T = 873\ °C$	$T = 878\ °C$	$T = 883\ °C$
X_K	0.691	0.640	0.617	0.650	0.611
r (1/min)	0.798	0.9081	0.868	0.491	0.292
t_0 (min)	34.330	34.974	37.790	44.040	53.576

$$\frac{dX}{dt} = f(X)r(T, P) \tag{12}$$

where $f(X)$ is a mechanistic-rate function that takes into account solids' heterogeneities.[52] Our experimental results on the time evolution of conversion (Figure 1) show the typical sigmoidal shape of autocatalytic processes and are well fitted by a Prout–Tompkins model function $f(X) = X(1 - X)$[53] modified by introducing a conversion limit X_K, which is the CaO conversion at the end of the reaction controlled phase (after which carbonation becomes controlled by solid-state diffusion of CO_2 across de $CaCO_3$ layer built up on the CaO surface). Thus

$$\frac{dX}{dt} = X\left(1 - \frac{X}{X_k}\right)r(T, P) \leftrightarrow X(t) = \frac{X_k}{1 + e^{-r(t-t_0)}} \tag{13}$$

Equation 13 fits quite satisfactorily to our experimental data on CaO conversion (Figure 1), which allows us deriving experimental values for the reaction rate at different temperatures $r(T, P)$. Best fitting parameters are shown in Table 1. Reaction rates obtained in this way are compared to the theoretically predicted values (eq 6) in Figure 2. It should be noted that while the modified Prout–Tompkins model used here provides a good fitting to experimental data, it has been shown in the literature that the kinetics parameters, i.e. activation energy, obtained from the analysis of isothermal data, is independent of the assumed kinetic model, and in any case, it leads to the real value of the activation energy.[54]

As may be seen in Figure 2a, a rather good agreement can be found between experiments and theory (eq 6) by only adjusting the prefactor a_2 as a free parameter in the theoretical curve. Interestingly, data obtained using different commercial thermal analysis instruments with quite different experimental setups could be nicely fitted by eq 6. In view of these results, and even though technical limitations prevented us from carrying out carbonation experiments at pressures greater than atmospheric, we will use eq 6 and its approximate limit (eq 10) to estimate the reaction rate under CO_2 at pressurized conditions (predicted curves are shown in Figure 2b).

Table 2 summarizes the values used for the reaction enthalpies, entropies, and activation energies, as discussed in the previous section, that will be employed for the theoretical reaction rate in the modeling analysis ahead.

As seen in Figure 2b, there is a temperature at which the carbonation rate reaches a maximum and above which it rapidly decreases as the equilibrium temperature is approached. This same trend was already predicted by Kyaw et al.[41] The temperature at which the reaction rate is maximum is a relevant input for the CaL-CSP application. Plant efficiency will be higher the higher the carbonation temperature, but considering that temperatures nearby equilibrium affects negatively to kinetics. The plot in Figure 3 shows the equilibrium temperature and temperature at which the reaction rate is maximum for carbonation under pure CO_2 as a function of the absolute carbonator pressure calculated from the carbonation kinetics model developed above.

A further interesting parameter derived from the best fit of eq 13 to experimental data on conversion is X_K, namely the value of CaO conversion at the boundary between the fast reaction and solid-state diffusion stages. Values for the conversion at the end of the reaction-controlled stage X_K obtained in this way are shown in Figure 4.
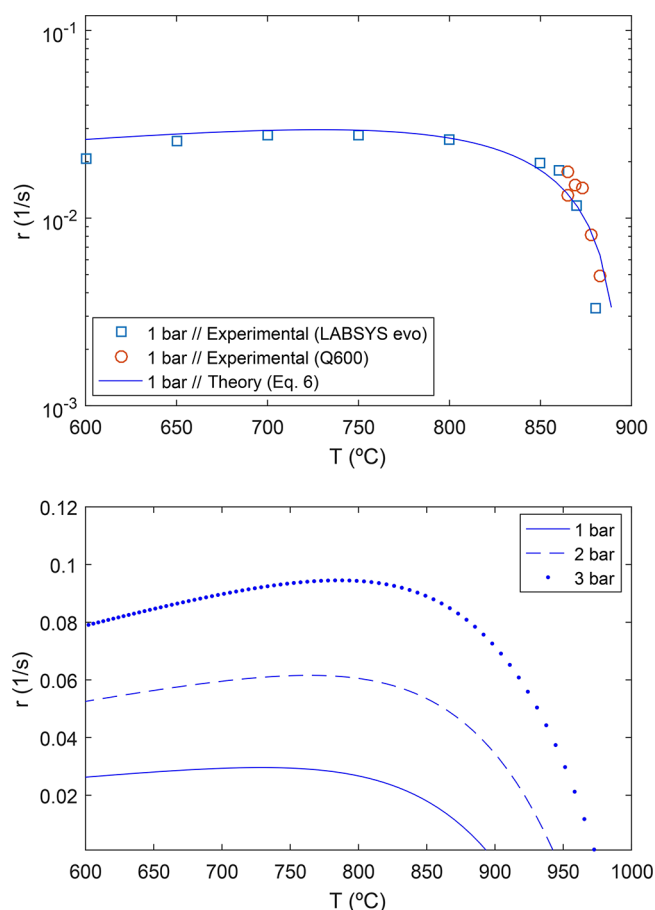

Figure 2. (top) Reaction rate obtained from experimental tests (using different TG analyzers as indicated) and theoretically predicted (eq 6, with $a_2 = 1160$ 1/s) for carbonation under pure CO_2 at atmospheric pressure as a function of the temperature. (bottom) Reaction rate as a function of temperature theoretically predicted by varying the carbonator absolute pressure (eq 6).

■ CARBONATOR MODEL

TGA Data Analysis. The behavior of CaO conversion X along multiple calcination/carbonation cycles is a critical input for the CaL cycle assessment. The CaL process applied to postcombustion CO_2 capture involves carbonation under low CO_2 partial pressure (around 0.15 bar for coal fired power plants) whereas calcination is carried out under high CO_2 concentration at temperatures around 950 °C. These harsh calcination conditions lead to a severe decay of CaO conversion in short residence times with the number of cycles due to progressive sintering of the regenerated CaO and the consequent drop of available surface area for carbonation in the fast reaction controlled stage.[55] Thus, conversion of limestone derived CaO in short residence times (of a few minutes) decays significantly after just a few cycles at CaL conditions for CO_2

Table 2. CO$_2$ Values of Enthalpy−Entropy Changes in the Chemical Decomposition and Desorption Stages and Activation Energies

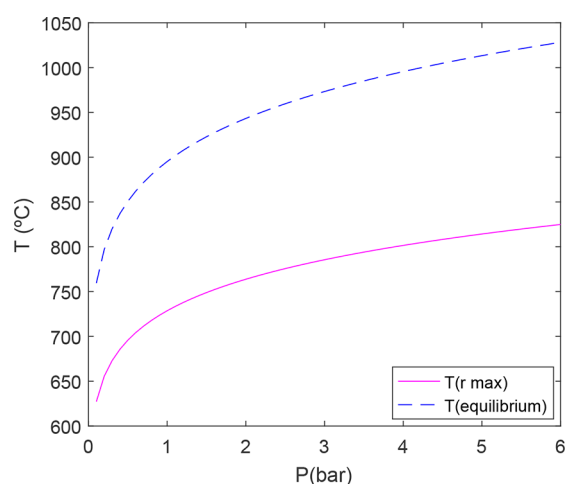|	
ΔH_r^0	180 kJ/mol
ΔH_1^0	160 kJ/mol
ΔH_d^0	20 kJ/mol
E_d	20 kJ/mol
E_1	180 kJ/mol
E_2	20 kJ/mol
ΔS_r^0	0.16 kJ/(mol·K)
ΔS_1^0	0.068 kJ/(mol·K)
ΔS_d^0	0.092 kJ/(mol·K)
a_2	1160 (1/s)

Figure 3. Values of temperature at which the carbonation reaction rate is maximum calculated from the kinetics model and at which the reaction is at equilibrium (carbonation under pure CO$_2$) as a function of the carbonator absolute pressure.
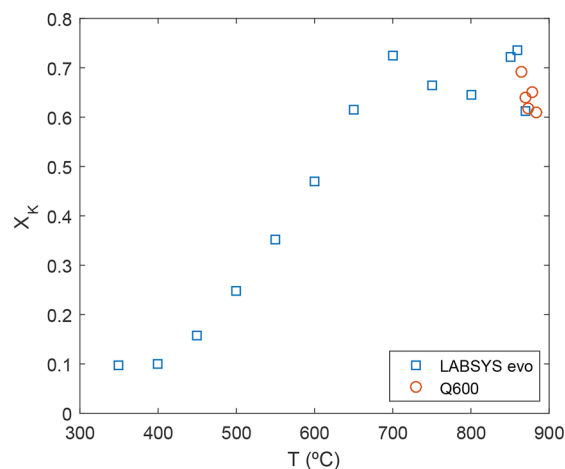

Figure 4. CaO conversion at the end of the reaction-controlled stage (X_K) for carbonation under pure CO$_2$ (at atmospheric pressure) as a function of temperature. Data are obtained from the best fits of eq 13 to experimental data on the time evolution of conversion.

capture and converges toward a residual value of just around 0.07−0.08.[26,55] Moreover, part of the CaO is irreversibly sulfated or deactivated by ashes. A number of methods to enhance the multicycle CaO conversion have been reported in the last years,[27] such as the formulation of synthetic sorbents,[56,57] thermal pretreatment,[58,59] mechanical pretreatment,[60] and

using steam or helium in either the calcination or carbonation reactors.[32,61]

However, CaL conditions for TCES in CSP do not need to be identical to those employed for CO$_2$ capture. In previously proposed CaL-CSP integration schemes[12,31,62] carbonation is carried out under a pure CO$_2$ atmosphere whereas calcination can be carried out under low CO$_2$ partial pressure, which leads to a different multicycle behavior.[37] Moreover, SO$_2$ and ashes are not present in the reactors. Thus, the residual conversion of limestone derived CaO can be as large as 0.5 for carbonation under 100% CO$_2$ atmosphere and calcination at 725 °C in absence of CO$_2$ for residence times in both stages of 5 min and using limestone particles smaller than 45 μm.[35] Carbonation under these conditions is limited by pore plugging, which leads to a significant loss of activity for typical particle sizes to be employed in circulating fluidized beds (>100 μm).[37] Thus, pore plugging causes a drop of the residual conversion of limestone derived CaO to just about $X = 0.2$ for particles larger than about 45 μm. Nevertheless, it has been reported that pore plugging does not limit carbonation for large enough dolomite particles (>∼100 μm) reaching a residual effective conversion of about 0.4.[37]

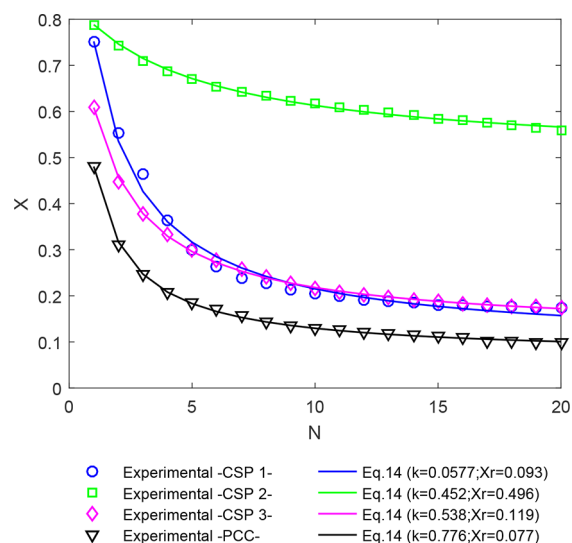Figure 5 shows thermogravimetric experimental data (see refs 35 and 37 for further details) on the multicycle conversion

Figure 5. Thermogravimetric experimental data[35,37,65] on the multicycle conversion (X) of limestone derived CaO under typical calcination/carbonation conditions for postcombustion CO$_2$ capture (PCC) and thermochemical energy storage of CSP. Testing conditions are shown in Table 3. The lines are the best fit curves from eq 14 to data. Best fitting parameters are shown in the legend.

of limestone derived CaO for several carbonation/calcination conditions. Testing conditions (particle size range used, type of atmosphere, temperature, and residence time in both calcination and carbonation stages) are detailed in Table 3. As can be seen, the evolution of CaO conversion X with the number of cycles N is well-fitted by eq 14:[63]

$$\frac{X_N}{X_1} = \frac{X_r}{X_1} + \left(\frac{1}{\kappa(N-1) + \left(1 - \frac{X_r}{X_1}\right)^{-1}} \right) \quad (14)$$

where X_1 is CaO conversion in the first cycle, k is the deactivation rate constant, and X_r is the residual CaO conversion,

Table 3. TGA Test Conditions Corresponding to Measured Multicycle CaO Conversion Data Plotted in Figure 5

reference	particle size	gas calciner−carbonator	temperature calciner−carbonator
CSP 1	>45 μm	He−CO_2	725−850 °C
CSP 2	<45 μm	He−CO_2	725−850 °C
CSP 3	>45 μm	CO_2−CO_2	950−850 °C
PCC	>45 μm	CO_2−N_2/CO_2 (15% v/v)	950−650 °C

which would be reached asymptotically after a very large number of cycles (as would occur in commercial CaL plants).

As shown in Figure 5, a higher CaO deactivation occurs for postcombustion CO_2 capture (PCC) conditions compared to CaL-CSP conditions. Thus, after 20 cycles, CaO conversion drops to 0.1 whereas under CaL-CSP3 conditions (calcination at 950 °C and carbonation at 850 °C, both under pure CO_2) conversion after 20 cycles remains at 0.18. A similar value of the residual conversion for CaO derived limestone is reported by Obermeier et al.,[64] who performed calcination at 800 °C in an air atmosphere and carbonation at 600 °C under a pure CO_2 atmosphere.

Carbonator Model. A carbonator model, previously employed to analyze the CaL process for CO_2 capture,[66] has been adapted in this work to study the CaL process for its integration in CSP plants. The model conforms to the flow diagram shown in Figure 6. The flow rate of CaO solids entering the carbonator (F_R) as well as the CaO present in the reactor bed (N_{Ca}) react with the pure CO_2 stream (flow rate F_{CO2}) to produce $CaCO_3$. As discussed above in the kinetics study, CaO conversion for a single particle in a certain residence time is dependent on carbonation temperature (Figure 1). Moreover, CaO conversion after several cycles decays close to a residual value, which is also dependent on process conditions. Thus, since carbonation is not completely achieved in short residence times, only a fraction of the total CaO flow rate (given by CaO conversion X) reacts to produce $CaCO_3$, the rest $(1 - X)$ remaining as unreacted CaO ($F_{CaO,unr}$). The model assumes a perfect mixing of solids in the reactor bed with a CO_2 stream passing in plug flow through it. At the carbonator exit, the CO_2 mass flow rate is decreased according to the CO_2 captured in the process (with an efficiency E_{CO2}).

By means of a mass balance, the maximum average conversion of the CaO particles in the carbonator can be expressed as

$$X_{\mathrm{max,ave}} = \sum_{N=1}^{N=\infty} \phi_N X_N \tag{15}$$

Here X_N is the average CaO conversion at cycle N and ϕ_N is the fraction of solids that are cycled N times:[67]

$$\phi_N = \frac{F_0 F_R^{N-1}}{(F_0 + F_R)^N} \tag{16}$$

where F_0 is the flow rate of makeup fresh limestone introduced to the system in order to mitigate CaO deactivation. If this fresh material is not introduced into the system, the maximum conversion after many cycles would be just the residual CaO conversion ($X_{\mathrm{max,ave}} \approx X_r$).

As is well-known from previous works,[38,67−69] carbonation takes place through two differentiated stages, a first fast stage in which the reaction occurs on the free surface of CaO particles (see reaction mechanism in the Carbonation Kinetics section) and a second stage, that takes place once a carbonate layer has been formed on the particles' surface, controlled by counter-current diffusion of CO_3^{2-} and O^{2-} across the $CaCO_3$ product layer and characterized by a much lower reaction rate. According to previous TGA studies, after calcination at 725 °C, most of the carbonation in short residence times on the regenerated CaO skeleton occurs in the fast stage due to the high CO_2 concentration and carbonation temperature, which promote the reaction kinetics.[37] Thus, carbonation in the diffusion-controlled phase is neglected in this model,[35] and therefore, $X_r = X_K$.

Accordingly, the present carbonator model assumes that carbonation occurs at a given rate until it reaches the maximum carbonation allowed in the fast carbonation stage, after which the particles remain inactive. Thus, only a fraction of particles, f_a, are active in the carbonator with the capacity to react in the fast reaction controlled stage:

$$f_a = (1 - e^{-t_K/\tau}) \tag{17}$$

where t_K is the fast carbonation stage time and τ is the average residence time of CaO solids in the carbonator:

$$\tau = \frac{N_{Ca}}{F_R} \tag{18}$$
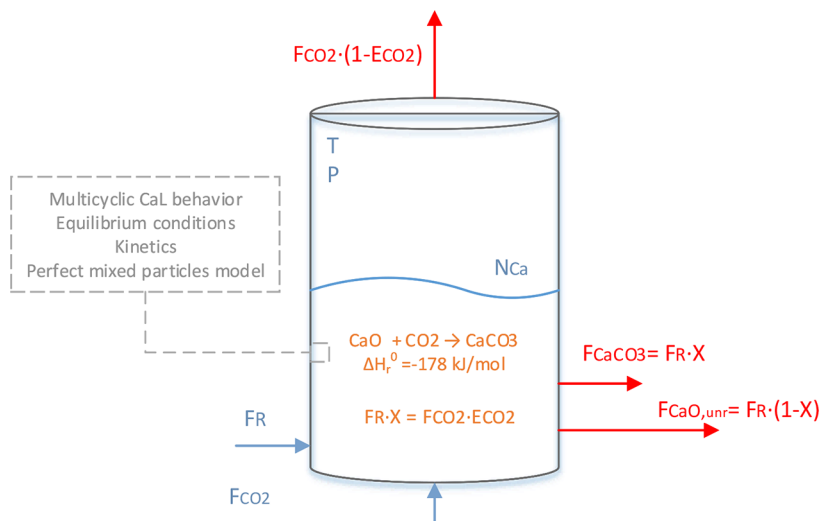
Figure 6. Carbonator model flow diagram.

Considering a perfect mixing model, the average conversion of the particles leaving the carbonator (X) can be calculated using the followed equations:[66]

$$X = \frac{\int_0^{t_K} r_{ave} t \left(\frac{1}{\tau}\right) e^{-t/\tau} \, dt}{1 - e^{-t_K/\tau}} = X_{max,ave} \frac{f_a}{\ln\left(\frac{1}{1-f_a}\right)} \tag{19}$$

$$f_{carb} = \frac{X}{X_{max,ave}} \tag{20}$$

$$E_{CO2} = \frac{F_R}{F_{CO2}} X = \frac{N_{Ca} f_a r_{ave}}{F_{CO2}} \tag{21}$$

where f_{carb} is the average carbonation level in the carbonator and r_{ave} is the average reaction rate in the fast carbonation stage, which is calculated from the kinetics model theoretical prediction (eq 10).

The carbonator model allows us to carry out a sensitivity analysis to assess the effect of pressure, temperature and solids inventory in the carbonator on the average carbonation level (f_{carb}). Results are shown in Figure 7.
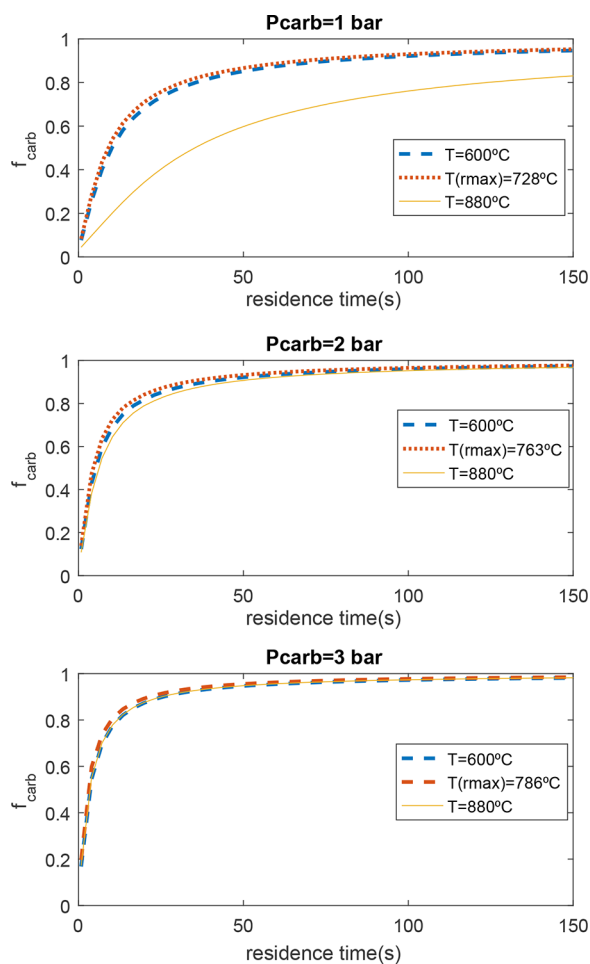

Figure 7. Carbonator model results. Average carbonation level (f_{carb}) for several carbonation conditions (P, T). T(rmax) is the temperature at which the reaction rate reaches a maximum (Figure 3).

As can be seen in Figure 7, the average carbonation level (f_{carb}) is enhanced by increasing the carbonator pressure due to faster reaction kinetics (Figure 2b). After a few of seconds in

the carbonator, most of the CaO reaches the maximum conversion (according to eq 13) due to the very fast kinetics achieved in these CaL conditions. This is basically because of the high amount of CO_2 entering the carbonator (which exceeds the stoichiometric amount in order to use the effluent excess as heat carrier). According to the kinetics model, by increasing the carbonator temperature, the average carbonation level is slightly enhanced up to the temperature T(rmax)—Figure 3—is reached from which kinetics is penalized with the consequent curtailment of the average carbonation level. As shown in Figure 7, this effect is mitigated when the carbonator pressure is increased, which is beneficial in practice since working at higher carbonator temperatures will promote the power cycle efficiency. Next section analyses the CSP-CaL integration efficiency as a function of carbonator temperature and pressure in order to select the best conditions based on both experimental data and the theoretical reaction kinetics study.

CSP-CaL Plant. This section is devoted to a detailed analysis on the CSP-CaL integrated plant for TCES. As main novelties regarding previous works,[12,70] new CaL conditions, TGA experimental data and the carbonator model above-described will be introduced in the analysis. Calculations have been performed using the commercial software Aspen PlusTM.

The CSP-CaL plant (see Figure 8) works as follows: Direct solar irradiation is used to preheat the streams entering the calciner up to the reaction temperature to carry out the calcination reaction. Calcination occurs under helium atmosphere which allows reducing the calcination temperature to 725 °C[33] in short residence times to simulate conditions as tested in the Carbonation Kinetics section using limestone as a CaO precursor. Note that the proposed scheme (Figure 8) is a closed cycle in which any stream must be fed continuously to the plant. This is relevant for the recycling of helium in the system, which is a rare and expensive gas. Several solar calciner reactors have been already proposed in the literature.[71−74] By calcination under an He atmosphere, a reduction of the calcination temperature would lead to an increase in the solar receiver efficiency as a consequence of the lower radiative losses. Full calcination is assumed in our model.[64,75] After calcination, the CaO stream ($c1$ in Figure 8) is separated from the He-CO_2 stream ($g1$) by means of a cyclone. The He−CO_2 stream is passed through a separation system based on membranes. A detailed study on the membrane system is out of the scope of this work and an ideal separation is assumed. However, it may be noted that commercial H_2/CO_2 separation membranes are available, and since He molecule is similar to H_2, the He/CO_2 separation system could take advantage of H_2/CO_2 currently commercial technologies. The He stream ($g1$-2) is recirculated into the calciner while the pure CO_2 stream ($g1$-1) is passed through a heat recovery steam generator (HRSG) to use its high temperature as a previous step to be stored or used in the power cycle. Since heat input to the steam power cycle is moderate, a simple superheated steam cycle without reheat stages and moderate live steam conditions are assumed. Thus, the steam cycle is modeled by considering a condensing pressure of 0.075 bar, an evaporation pressure of 45 bar and a superheated steam temperature of 400 °C.

On the carbonator side of the plant, a CaO stream from the storage vessel (c_2) reacts with the CO_2 stream coming either from storage ($g7b$) or the calciner side ($g3$) according to the carbonation reaction at atmospheric pressure (carbonation at higher pressure will be also considered ahead). The CO_2 entering the carbonator ($g9$-2) exceeds the stoichiometric amount
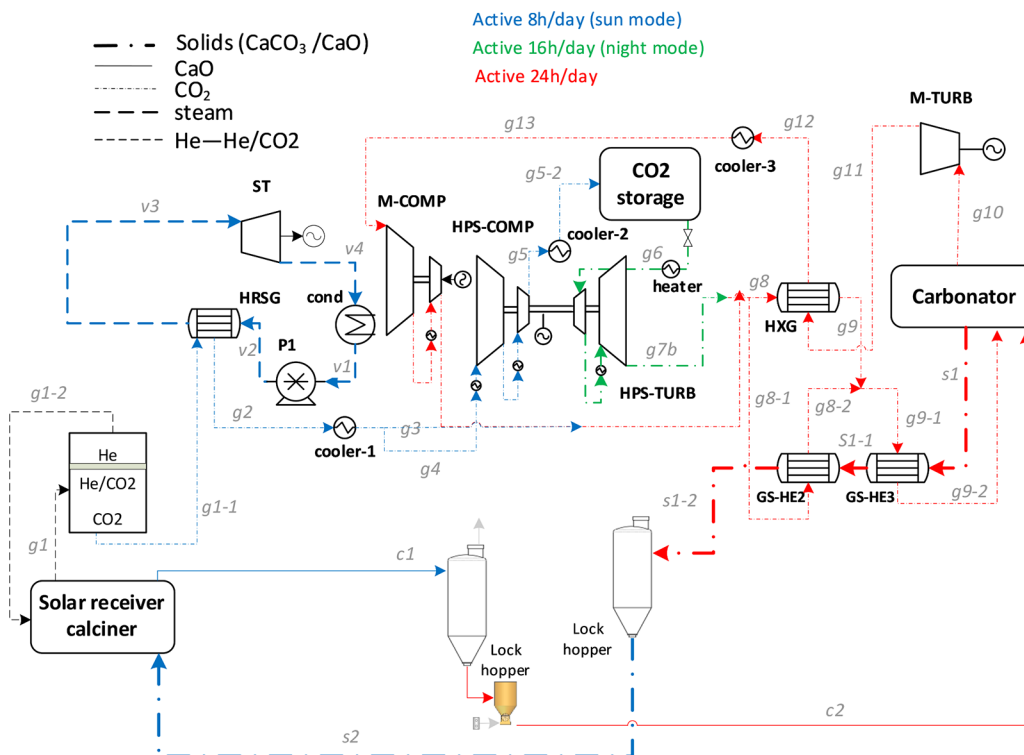
Figure 8. CSP-CaL plant scheme.

needed for carbonation. The CO_2 in excess that exits the carbonator acts as heat carrier to produce electrical power by means of a CO_2 closed Brayton cycle wherein a heat exchanger HXG is used as a recuperator.

Different operations in "sun" and "night" modes are simulated. A solar multiple (SM) equal to 3 is assumed for the system design and, for simplicity, the day is considered as composed by 8 sun h, which constantly provides 100 MWth to the calciner, and of 16 night h. Thus, in the "sun" operating mode, the CO_2 mass flow entering the carbonator side (g3 or g7b) is 1/3 the amount produced in the calciner (g1). Accordingly, the plant efficiency is determined as a weighted average of the performances in sun and night modes (eq 22). Although it is out of the scope of the present work, an additional analysis to consider real solar irradiance as well as off-design conditions would be required for further assessing equipment sizing and costs. Moreover, other plant operation modes could be considered as a function of solar irradiation, electricity prices, filling level of storage tanks, etc. On the other hand, a more detailed study on the different operation modes would be useful to estimate the penalty associated with daily start-up/shut-down of the plant. In this regard, lower start-up/shut-down penalties than in commercial CSP plants are expected since the system is designed to achieve a full working hours capacity. Note that efficiency in this model considers the heat input to the calciner and disregards the thermal efficiency of the solar receiver whose design and modeling is beyond the scope of this work. Concerning solids transport, a power consumption of 20 MJ/ton is assumed.[12] Thus, the global plant efficiency will be given by

$$\eta = \frac{\int_{24h} \dot{W}_{net} \, dt}{\int_{24h} \dot{Q}_{input} \, dt} = \frac{\dot{W}_{net,sun}\Delta t_{sun} + \dot{W}_{net,night}(24 - \Delta t_{sun})}{\dot{Q}_{input}\Delta t_{sun}}$$

(22)

where $\dot{W}_{net}$ is the net electrical power produced by the system and $\dot{Q}_{input}$ is the solar power input in the calciner. The electric power produced is computed for the sun mode ($\dot{W}_{net,sun}$) and the night mode ($\dot{W}_{net,night}$).

Several assumptions have been made to model the CSP-CaL plant, which are summarized in Table 4.

CSP-CaL Integration Model Results. The proposed CSP-CaL integration model has been simulated considering in the base case that the carbonator works at 850 °C/1 bar and with a solids inventory of 105 kmol, which allows to achieve a 95% of average carbonation level (f_{carb}) in the carbonator (Figure 7). An important benefit of working at atmospheric pressure in the carbonator is that high temperature lock hoppers for solids pressurization are not necessary. On the other hand, hermetic machines and heat exchangers must be employed. Tables 5 and 6 show the main streams and energy balance results.

The energy balance for the CSP-CaL integration shows an overall daily efficiency of 38% (Table 6). Since the main turbine (M-TURB) has been selected to work at constant power production, a higher net power output is achieved during the night mode compared to the sun mode. This is because the high-pressure CO_2 storage compressor (HPS-COMP) and auxiliaries' consumptions are not fully compensated by the steam turbine production in the sun mode. As shown in Table 6, main heat rejections to the ambient occur in the steam condenser (COND) and in the CO_2 cycle precooler (COOLER-3) while the main power consumption is caused by the CO_2 compressor in the carbonator side (M-COMP).

The CSP-CaL integration performance has been analyzed as a function of the pressure ratio (PR) defined as the ration of the carbonator pressure (1 bar) to the turbine outlet pressure. On one hand, by increasing the pressure ratio the power production in the CO_2 power cycle is enhanced, which increases the global cycle efficiency. On the other hand, by increasing PR, the temperature of the CO_2 exiting the turbine is lowered and a

Table 4. Main Assumptions in the CSP-CaL Model

group/component	parameter		
turbomachinery	isentropic efficiency	mechanical-electric efficiencies	intercooling/reheating stages and temperatures
main CO_2 turbine (M-TURB)	0.9	0.98	
main CO_2 compressor (M-COMP)	0.87	0.98	2/40 °C
high pressure storage turbine (HPS-TURB)	0.8	0.96	2
			65 °C/100 °C
high pressure storage compressor (HPS-COMP)	0.8	0.96	5/40 °C
steam turbine (ST)	0.75	0.98	

component	parameter		
heat exchangers	minimum temperature difference	pressure drops	parasitic power consumption
coolers	15 °C	1%	0.8% of heat released[76]
HXG (both sides)	15 °C	5%	
HRSG (hot side)	15 °C	3%	
HRSG (cold side)	15 °C	11%	
solid−gas HX (both sides)	15 °C	3%	

component	parameter		
various	efficiency	heat input	heat losses
calciner	1	100 MWt	
carbonator			1% of heat transferred
storage vessels			0%

higher amount of energy is recovered in the recuperator (HXG), which translates into a higher amount of carbonation energy needed to bring the reactants to carbonation conditions. The effect of increasing the PR on the overall plant efficiency is illustrated in Figure 9.

As can be seen in Figure 9, a higher overall efficiency is calculated as the carbonation temperature is increased at a given value of PR. Thus, the benefits of increasing the carbonation temperature above $T_{carb} \sim 728$ °C (at which the reaction rate is maximum for atmospheric carbonation as shown in Figure 2b) compensates the penalty caused by the reduction of the reaction speed which yields a lower carbonation level and therefore a lower CaO conversion (X).

Table 6. Energy Balance for the CSP-CaL Integration (Figure 8)

parameter	sun mode	night mode
solar thermal power (MWth)	100	0
Heat Exchanger Thermal Power (MWth)		
HRSG	16.01	
COOLER-1	−0.37	
COND	−11.68	
HP-COMP (intercooler)	4.50	
COOLER-2	−4.01	
HEATER	2.07	
TURB1 (interheater)	-	0.97
COOLER-3	-	−5.63
HXG	88.81	88.81
GS-HE2	3.602	3.602
GS-HE3	4.782	4.782
Power Inlet (MWe)		
CO_2 storage turbine (HPS-TURB)		1.32
main CO_2 turbine (M-TURB)	25.35	25.35
steam turbine (ST)	4.27	
Power Outlet (MWe)		
steam cycle pump (P)	−0.03	
main CO_2 compressor (M-COMP)	−12.59	−12.50
CO_2 storage compressor (HPS-COMP)	−5.14	
auxiliaries heat calciner	−0.16	
auxiliaries heat carbonator	−0.11	−0.16
auxiliaries solids transport calciner	−0.87	
auxiliaries solids transport carbonator	−0.29	−0.29
Wnet		
$\dot{W}_{net,sun}$ (MWe)	10.42	
$\dot{W}_{net,night}$ (MWe)		13.77
overall plant efficiency (η)	38%	

The temperature limit imposed by the thermodynamic equilibrium (eq 8) for carbonation under pure CO_2 at atmospheric pressure is 895 °C (Figure 3). Thus, the carbonator pressure must be increased over atmospheric pressure to further increase the carbonator temperature above 895 °C. This would enhance the power plant efficiency (higher temperature at turbine inlet) as well as the carbonation kinetics (as shown in Figure 2a and Figure 7). The CSP-CaL integration (Figure 8) is also valid when the carbonator is operated under over atmospheric pressure. For that purpose, the only modification needed is that the
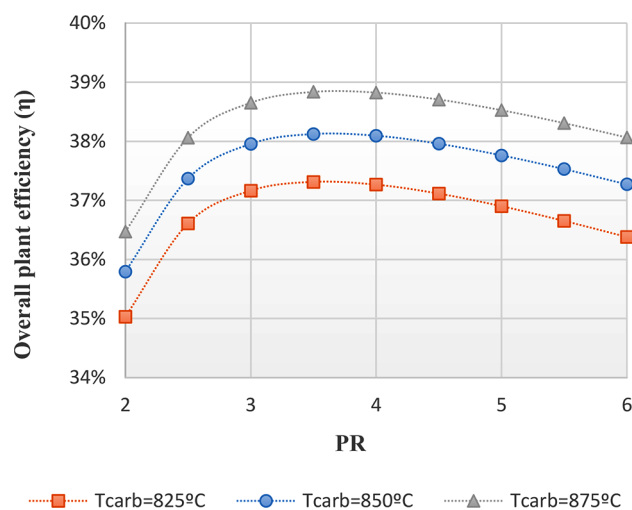
Table 5. Main Stream Data for the CSP-CaL Integration (Base Case)

ID	P (bar)	T (°C)	$\dot{m}$ (kg/s)	ID	P (bar)	T (°C)	$\dot{m}$ (kg/s)
s1	1.00	850	29.13	g4	1.14	44.43	14.69
s1-1	0.97	703.17	29.13	g5	75.75	123.63	14.69
s1-2	0.94	588.83	29.13	g5-2	75	25	14.69
s2	0.94	588.83	87.37	g6	74.25	130	7.34
c1	1.00	725	65.39	g7b	1.14	21.92	7.34
c2	1.00	725	21.79	g8	1.14	72.10	134.62
v1	0.074	40.13	5.27	g8-1	1.14	72.10	6.54
v2	45.00	40.53	5.27	g8-2	1.10	535.06	6.54
v3	40.00	400	5.27	g9	1.08	679.56	134.62
v4	0.075	40.31	5.27	g9-1	1.08	675.41	141.17
g1	1.00	725	440.58	g9-2	1.05	703.17	141.17
g1-1	1.00	725	22.03	g10	1.00	850	133.82
g1-2	1.00	725	418.55	g11	0.33	694.56	133.82
g2	0.97	58.99	22.03	g12	0.32	87.30	133.82
g3	1.14	44.43	7.34	g13	0.31	40	133.82

Figure 9. Overall plant efficiency as a function of pressure ratio (PR).

CO_2 stream coming from the calciner (g3 stream in Figure 8) in the day mode is passed through the main CO_2 compressor (M-COMP) up to reach the carbonator pressure (including the pressure drop) as a previous step to enter the recuperator (HXG). Note that the CO_2 exiting the main turbine (M-TURB) can be at atmospheric pressure working under pressurized carbonation conditions. Therefore, hermetic machines and heat exchangers would not be necessary. Figure 10 shows the overall
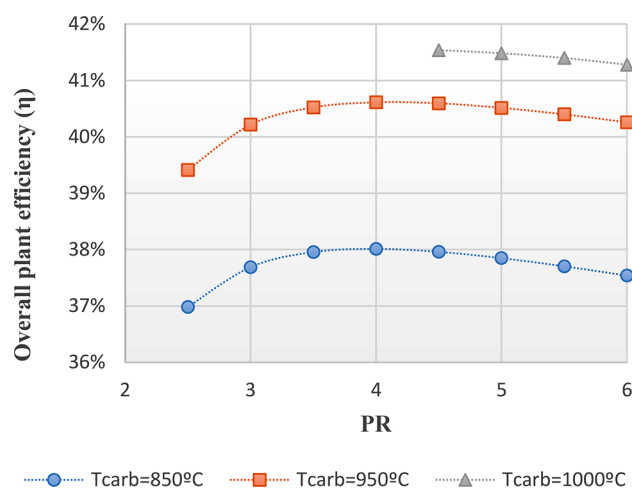

Figure 10. Overall plant efficiency as a function of the pressure ratio (PR) for carbonation at over atmospheric pressure (P_{carb}). The CO_2 exiting the turbine (M-TURB) is at atmospheric pressure, and therefore P_{carb} = PR.

CSP-CaL efficiency for the pressurized carbonator case. Except for the carbonator conditions (P, T), the rest of the parameters are the same as in the base case.

By comparing Figures 9 and 10 it is appreciated that the overall plant efficiency is significantly enhanced by increasing the carbonator temperature, which is facilitated when the carbonator works under pressurized conditions. In this way, overall plant efficiencies above 41% are achievable. Note that in the case of T_{carb} = 1000 °C the carbonator pressure must be higher than 4.21 bar due to thermodynamic equilibrium constraints.

Carbonator Presizing. At this point an important issue regarding the carbonator size must be addressed. The carbonator in the application of the CaL technology for post-combustion

CO_2 capture (PCC) is characterized by a very large size (volume ∼ 18 m^3/MWe; solids inventory ∼ 1300 kg/MWe[77]), which significantly increases capital and operating costs (CAPEX and OPEX).[78,79] Previous works[80,81] have shown that the sizes of the carbonator and calciner play an important role on increasing the cost of the PCC technology. In contrast, the carbonator size in the application of the CaL technology for TCES in CSP would be remarkably reduced as evidenced by stream data (Table 5). Table 7 shows the carbonator reactor presizing for

Table 7. Carbonator Reactor Properties in the CSP-CaL Integration (Base Case)

parameter	base case (P_{carb} = 1 bar)	pressurized carbonation (P_{carb} = 3 bar)
power plant size (MW_{th})	100	100
Carbonator Operating Conditions		
P_{carb} (bar)	1	1
T_{carb} (°C)	850	950
$F_{R,crb}$ (kmol/h)	1399	1499
$F_{CO2crb,in}$ (kmol/h)	11547	10533
F_R/F_{CO2}	0.12	0.14
$\dot{V}_{CO2}$ (m^3/s)	248.5	85.44
W_s (kg)	8000	5000
Carbonator Preliminary Sizing		
reactor type	CFB	CFB
μ_0 (m/s)	4	4
particle size (μm)	100	100
A (m^2)	62.12	21.36
D (m)	8.89	5.21
W_s/A (kg/m^2)	128.78	234.08
H (m)	36.67	15.64

the case proposed in our study. Since gas and solids mass flow rates in the CSP-CaL case are relatively small, the cross-section surface area of the carbonator reactor (A ∼ 21 m^2 for the pressurized carbonator case) is small as compared to the typical size of the carbonator in the PCC-CaL application (A ∼ 175 m^2 [77]) assuming the same superficial velocity for the fluidized bed to be operated in a circulation regime. Likewise, the carbonator height, which can be estimated from the ratio a H/D ∼ 3[77] is much smaller in the CSP-CaL technology as compared to the PCC-CaL application.

The minimum amount of solids inventory needed can be estimated to achieve a 95% of average carbonation level in the carbonator while carbonation kinetics can be inferred from the Carbonation Kinetics section of this manuscript. As shown in Table 7, a solids inventory of ∼128−234 kg/MWe is needed, which is significantly lower than in the case of the PCC-CaL application (∼1300 kg/MWe). A direct consequence of a reduction in solids inventory in the carbonator, is a significant reduction of fan power consumption to ensure fluidization conditions. As would be expected, the base case requires a larger carbonator size as compared with the pressurized carbonator configuration. The atmospheric pressure carbonator in the base case involves a larger amount of CO_2 volume entering the reactor as well as a lower reaction rate, which would be enhanced with the carbonator pressure (Figure 2b).

■ CONCLUSIONS

This paper analyzes the carbonation of limestone derived CaO in the CaL process as for thermochemical energy storage in CSP plants. Since the carbonation behavior (kinetics and

multicyclic CaO conversion) is highly dependent on the CaL conditions, which vary according to the type of application, a theoretical reaction kinetics study has been carried out to analyze the effect of the particular CaL carbonation conditions to be used in the CSP-CaL integration, which involve carbonation under high CO_2 partial pressure at high temperature. The reaction kinetics study is supported by TGA tests performed under these specific conditions. As a result, a new expression to estimate the carbonation conversion rate as a function of the carbonator pressure and temperature has been derived. A carbonator model based on the kinetics study is used to estimate the average carbonation level after a long number of cycles as would occur at industrial scale. Accordingly, the carbonation rate is enhanced with the carbonator temperature up to reach a maximum, from which a further increase of temperature is detrimental as the thermodynamic equilibrium temperature is approached. On the other hand, an increase in the carbonator pressure promotes significantly the conversion rate and therefore the average carbonation level in short residence times. Thus, an increase of the carbonator pressure yields an improved performance not only from a reaction kinetics perspective but also because a higher carbonator pressure allows for a higher carbonator temperature, which enhances the power cycle efficiency when stored energy is released. The CSP-CaL integration model explored in this work, which is based on power production by means of a closed CO_2 Brayton cycle, shows that the overall plant efficiency is significantly promoted as the carbonator temperature is increased. Thus, optimum carbonator pressures are in the range of ~3.5−4 bar, which allow carbonator operation temperatures of 950 °C to yield global efficiencies of about 41%. As a final comment, it is remarkable that a fundamental understanding of physicochemical processes at the molecular level helped us tackle the industrial process with an extra degree of confidence.

■ AUTHOR INFORMATION

Corresponding Author
*Tel.: +34 655783930. E-mail address: cortiz7@us.es.
ORCID Ⓓ
C. Ortiz: 0000-0002-7795-676X
J. M. Valverde: 0000-0002-2345-8888
Notes
The authors declare no competing financial interest.

■ ACKNOWLEDGMENTS

■ NOTATION

A = carbonator cross-section, m^2
D = carbonator diameter, m
E_1 = activation energy for chemical decomposition, kJ/mol
f_a = fraction of CaO that reacts in the carbonator in the fast stage

f_{carb} = average carbonation level
F_i = molar flow rate of component i, kmol/s
F_{CaCO_3} = $CaCO_3$ molar flow rate
$F_{CaCO_3,crb}$ = $CaCO_3$ molar flow rate (calciner side)
$F_{CaO,unr}$ = molar flow rate of unreacted CaO (calciner side)
$F_{CO_2,clc}$ = CO_2 molar flow rate at calciner outlet
$F_{CO_2,crb,in}$ = CO_2 molar flow rate at carbonator inlet
$F_{CO_2,crb,out}$ = CO_2 molar flow rate at carbonator outlet
F_O = mole flow rate of fresh makeup limestone, kmol/h
F_R = mole flow rate of CO_2 in flue gas entering the carbonator, kmol/h
$F_{R,crb}$ = recirculating molar flow rate (carbonator side)
$F_{R,clc}$ = recirculating molar flow rate (calciner side)
h_i = enthalpy, kJ/kmol
H = carbonator height, m
$\dot{m}$ = mass flow rate, kg/s
N = cycle number
N_{Ca} = mol of Ca in the carbonator, mol
P = pressure, bar
P_{carb} = absolute carbonator pressure, bar
P_{eq} = CO_2 partial pressure at equilibrium, bar
PR = pressure ratio
$\dot{Q}_{input}$ = solar power input
r = reaction rate, s^{-1}
r_{ave} = average reaction rate, s^{-1}
SM = solar multiple
t = time, s
T = temperature, °C
$T_{calciner}$ = calciner temperature, °C
T_{carb} = carbonator temperature, °C
T_{eq} = equilibrium temperature, °C
t_k = fast carbonation stage time, s
μ_0 = mean superficial velocity in the CFB riser, m/s
$\dot{V}_{CO2}$ = CO_2 volume flow rate, m^3/s
W_s = solid inventory in the carbonator per MW of a typical power plant, kg
$\dot{W}_{net}$ = average electrical power, MWe
$\dot{W}_{net,night}$ = net electrical power for the night mode, MWe
$\dot{W}_{net,sun}$ = net electrical power for the sun mode, MWe
$\dot{W}_{M-TURB}$ = power produced by the main CO_2 turbine, MWe
$\dot{W}_{M-COMP}$ = power consumed by the main CO_2 compressor, MWe
$\dot{W}_{HPS-TURB}$ = power produced by the high-pressure CO_2 turbine, MWe
$\dot{W}_{HPS-COMP}$ = power consumption of high pressure intercooled CO_2 compressor for the storage system, MWe
$\dot{W}_{ST}$ = power produced in the steam turbine cycle, MWe
$\dot{W}_P$ = power consumed in the steam turbine cycle, MWe
$\dot{W}_{PSOLCAL}$ = power consumptions for solids transport in the calciner side, MWe
$\dot{W}_{PSOLCAR}$ = power consumptions for solids transport in the carbonator side, MWe
$\dot{W}_{AUXPOWCA}$ = auxiliary power consumptions in the calciner side, MWe
$\dot{W}_{AUXPOWCR}$ = auxiliary power consumptions in the carbonator side, MWe
X = average CaO conversion
X_{ave} = average conversion of the sorbent
$X_{max,ave}$ = maximum average conversion of the sorbent
X_K = CaO conversion in the fast carbonation stage
X_N = CaO conversion at the N cycle
X_r = residual CaO conversion
ΔP = pressure drop at carbonator, bar

ΔS_2^0 = carbonation entropy change, J/(mol·K)

Δt_{sun} = average daytime period, h

$\Delta H_r(T_{react})$ = reaction enthalpy at the reactor temperature, kJ/mol

ΔP = pressure drop at carbonator, bar

ΔS_2^0 = carbonation entropy change, J/(mol·K)

Δt_{sun} = average daytime period, h

$\Delta H_r(T_{react})$ = reaction enthalpy at the reactor temperature, kJ/mol

ΔH_r^0 = standard enthalpy of reaction, kJ/mol

η = overall net efficiency

κ = deactivation constant rate

τ = average residence time in the carbonator, s

ϕ_N = fraction of solids cycled N times

■ REFERENCES

(1) Gil, A.; Medrano, M.; Martorell, I.; Lázaro, A.; Dolado, P.; Zalba, B.; Cabeza, L. F. State of the Art on High Temperature Thermal Energy Storage for Power Generation. Part 1—Concepts, Materials and Modellization. *Renewable Sustainable Energy Rev.* **2010**, *14* (1), 31−55.

(2) Wagner, S. J.; Rubin, E. S. Economic Implications of Thermal Energy Storage for Concentrated Solar Thermal Power. *Renewable Energy* **2014**, *61*, 81−95.

(3) Denholm, P.; Wan, Y. Y. H.; Hummon, M.; Mehos, M. *An Analysis of Concentrating Solar Power with Thermal Energy Storage in a California 33% Renewable Scenario (Technical Report NREL/TP-6A20−58186)*; 2013.

(4) National Renewable energy laboratory (NREL). Concentrating Solar Power Projects https://www.nrel.gov/csp/solarpaces/ (accessed Apr 2, 2017).

(5) Kearney, D.; Kelly, B.; Herrmann, U.; Cable, R.; Pacheco, J.; Mahoney, R.; Price, H.; Blake, D.; Nava, P.; Potrovitza, N. Engineering Aspects of a Molten Salt Heat Transfer Fluid in a Trough Solar Field. *Energy* **2004**, *29* (5−6), 861−870.

(6) Vignarooban, K.; Xu, X.; Arvay, A.; Hsu, K.; Kannan, A. M. Heat Transfer Fluids for Concentrating Solar Power Systems − A Review. *Appl. Energy* **2015**, *146*, 383−396.

(7) Liu, M.; Steven Tay, N. H.; Bell, S.; Belusko, M.; Jacob, R.; Will, G.; Saman, W.; Bruno, F. Review on Concentrating Solar Power Plants and New Developments in High Temperature Thermal Energy Storage Technologies. *Renewable Sustainable Energy Rev.* **2016**, *53*, 1411−1432.

(8) Valverde, J. M.; Barea-López, M.; Perejón, A.; Sánchez-Jiménez, P. E.; Pérez-Maqueda, L. A. Effect of Thermal Pretreatment and Nanosilica Addition on Limestone Performance at Calcium-Looping Conditions for Thermochemical Energy Storage of Concentrated Solar Power. *Energy Fuels* **2017**, *31* (4), 4226−4236.

(9) Ho, C. K. A Review of High-Temperature Particle Receivers for Concentrating Solar Power. *Appl. Therm. Eng.* **2016**, *109*, 958−969.

(10) N'Tsoukpoe, K. E.; Liu, H.; Le Pierrès, N.; Luo, L. A Review on Long-Term Sorption Solar Energy Storage. *Renewable Sustainable Energy Rev.* **2009**, *13* (9), 2385−2396.

(11) Pardo, P.; Deydier, A.; Anxionnaz-Minvielle, Z.; Rougé, S.; Cabassud, M.; Cognet, P. A Review on High Temperature Thermochemical Heat Energy Storage. *Renewable Sustainable Energy Rev.* **2014**, *32*, 591−610.

(12) Chacartegui, R.; Alovisio, A.; Ortiz, C.; Valverde, J. M.; Verda, V.; Becerra, J. A. Thermochemical Energy Storage of Concentrated Solar Power by Integration of the Calcium Looping Process and a CO_2 Power Cycle. *Appl. Energy* **2016**, *173*, 589−605.

(13) Hanak, D. P.; Manovic, V.; Biliyok, C. Calcium Looping with Inherent Energy Storage for Decarbonisation of Coal-Fired Power Plant. *Energy Environ. Sci.* **2016**, *9*, 971−983.

(14) Abedin, A. H. A Critical Review of Thermochemical Energy Storage Systems. *Open Renewable Energy J.* **2011**, *4* (1), 42−46.

(15) Felderhoff, M.; Urbanczyk, R.; Peil, S. Thermochemical Heat Storage for High Temperature Applications − A Review. *Green* **2013**, *3* (2), 113−123.

(16) Kuravi, S.; Trahan, J.; Goswami, D. Y.; Rahman, M. M.; Stefanakos, E. K. Thermal Energy Storage Technologies and Systems for Concentrating Solar Power Plants. *Prog. Energy Combust. Sci.* **2013**, *39* (4), 285−319.

(17) Ortega-Fernández, I.; Calvet, N.; Gil, A.; Rodríguez-Aseguinolaza, J.; Faik, A.; D'Aguanno, B. Thermophysical Characterization of a by-Product from the Steel Industry to Be Used as a Sustainable and Low-Cost Thermal Energy Storage Material. *Energy* **2015**, *89*, 601−609.

(18) Barker, R. The Reactivity of Calcium Oxide towards Carbon Dioxide and Its Use for Energy Storage. *J. Appl. Chem. Biotechnol.* **1974**, *24* (4−5), 221−227.

(19) Flamant, G.; Hernandez, D.; Bonet, C.; Traverse, J.-P. Experimental Aspects of the Thermochemical Conversion of Solar Energy; Decarbonation of CaCO3. *Sol. Energy* **1980**, *24* (4), 385−395.

(20) Badie, J. M.; Bonet, C.; Faure, M.; Flamant, G.; Foro, R.; Hernandez, D. Decarbonation of Calcite and Phosphate Rock in Solar Chemical Reactors. *Chem. Eng. Sci.* **1980**, *35* (1−2), 413−420.

(21) Williams, R. Hydrogen Production. US 1938202 A, 1933.

(22) Shimizu, T.; Hirama, T.; Hosoda, H.; Kitano, K.; Inagaki, M.; Tejima, K. A Twin Fluid-Bed Reactor for Removal of CO_2 from Combustion Processes. *Chem. Eng. Res. Des.* **1999**, *77* (1), 62−68.

(23) Dean, C. C.; Blamey, J.; Florin, N. H.; Al-Jeboori, M. J.; Fennell, P. S. The Calcium Looping Cycle for CO_2 Capture from Power Generation, Cement Manufacture and Hydrogen Production. *Chem. Eng. Res. Des.* **2011**, *89* (6), 836−855.

(24) Charitos, a.; Hawthorne, C.; Bidwe, A. R.; Sivalingam, S.; Schuster, A.; Spliethoff, H.; Scheffknecht, G. Parametric Investigation of the Calcium Looping Process for CO_2 Capture in a 10kWth Dual Fluidized Bed. *Int. J. Greenhouse Gas Control* **2010**, *4* (5), 776−784.

(25) Arias, B.; Diego, M. E.; Abanades, J. C.; Lorenzo, M.; Diaz, L.; Martínez, D.; Alvarez, J.; Sánchez-Biezma, A. Demonstration of Steady State CO_2 Capture in a 1.7MWth Calcium Looping Pilot. *Int. J. Greenhouse Gas Control* **2013**, *18*, 237−245.

(26) Grasa, G. S.; Abanades, J. C. CO_2 Capture Capacity of CaO in Long Series of Carbonation/Calcination Cycles. *Ind. Eng. Chem. Res.* **2006**, *45* (26), 8846−8851.

(27) Perejón, A.; Romeo, L. M.; Lara, Y.; Lisbona, P.; Martínez, A.; Valverde, J. M. The Calcium-Looping Technology for CO_2 Capture: On the Important Roles of Energy Integration and Sorbent Behavior. *Appl. Energy* **2016**, *162*, 787−807.

(28) Sanchez-Jimenez, P. E.; Valverde, J. M.; Perez-Maqueda, L. A. Multicyclic Conversion of Limestone at Ca-Looping Conditions: The Role of Solid-Sate Diffusion Controlled Carbonation. *Fuel* **2014**, *127*, 131−140.

(29) Valverde, J. M.; Sanchez-Jimenez, P. E.; Perez-Maqueda, L. Calcium-Looping for Post-Combustion CO_2 Capture. On the Adverse Effect of Sorbent Regeneration under CO_2. *Appl. Energy* **2014**, *126*, 161−171.

(30) Hanak, D. P.; Anthony, E. J.; Manovic, V. A Review of Developments in Pilot-Plant Testing and Modelling of Calcium Looping Process for CO_2 Capture from Power Generation Systems. *Energy Environ. Sci.* **2015**, *8* (8), 2199−2249.

(31) Ortiz, C.; Chacartegui, R.; Valverde, J. M.; Alovisio, A.; Becerra, J. A. Power Cycles Integration in Concentrated Solar Power Plants with Energy Storage Based on Calcium Looping. *Energy Convers. Manage.* **2017**, *149*, 815−829.

(32) Berger, E. E. Effect of Steam on the Decomposition of Limestone. *Ind. Eng. Chem.* **1927**, *19* (5), 594−596.

(33) Valverde, J. M.; Medina, S. Reduction of Calcination Temperature in the Calcium Looping Process for CO_2 Capture by Using Helium: In Situ XRD Analysis. *ACS Sustainable Chem. Eng.* **2016**, *4* (12), 7090−7097.

(34) Valverde, J. M.; Medina, S. Limestone Calcination under Calcium-Looping Conditions for CO_2 Capture and Thermochemical

Energy Storage in the Presence of H₂O: An in Situ XRD Analysis. *Phys. Chem. Chem. Phys.* **2017**, *19* (11), 7587−7596.

(35) Sarrion, B.; Valverde, J. M.; Perejon, A.; Perez-maqueda, L. A.; Sanchez-jimenez, P. E. On the Multicycle Activity of Natural Limestone/dolomite for Cheap, Efficient and Non-Toxic Thermochemical Energy Storage of Concentrated Solar Power. *Energy Technol.* **2016**, *4*, 1013.

(36) Benitez-Guerrero, M.; Valverde, J. M.; Sanchez-Jimenez, P. E.; Perejon, A.; Perez-Maqueda, L. A. Multicycle Activity of Natural CaCO₃ minerals for Thermochemical Energy Storage in Concentrated Solar Power Plants. *Sol. Energy* **2017**, *153*, 188−199.

(37) Benitez-Guerrero, M.; Sarrion, B.; Perejon, A.; Sanchez-Jimenez, P. E.; Perez-Maqueda, L. A.; Manuel Valverde, J. Large-Scale High-Temperature Solar Energy Storage Using Natural Minerals. *Sol. Energy Mater. Sol. Cells* **2017**, *168* (March), 14−21.

(38) Bhatia, S. K.; Perlmutter, D. D. Effect of the Product Layer on the Kinetics of the CO₂-Lime Reaction. *AIChE J.* **1983**, *29* (1), 79−86.

(39) Grasa, G.; Murillo, R.; Alonso, M.; Abanades, J. C. Application of the Random Pore Model to the Carbonation Cyclic Reaction. *AIChE J.* **2009**, *55* (5), 1246−1255.

(40) Gupta, H.; Fan, L.-S. Carbonation−Calcination Cycle Using High Reactivity Calcium Oxide for Carbon Dioxide Separation from Flue Gas. *Ind. Eng. Chem. Res.* **2002**, *41* (16), 4035−4042.

(41) Kyaw, K.; Kubota, M.; Watanabe, F.; Matsuda, H.; Hasatani, M. Study of Carbonation of CaO for High Temperature Thermal Energy Storage. *J. Chem. Eng. Jpn.* **1998**, *31* (2), 281−284.

(42) Moore, W. J. *Physical Chemistry*, 5th ed.; Prentice-Hall, 1999.

(43) Pijolat, M.; Soustelle, M. Experimental Tests to Validate the Rate-Limiting Step Assumption Used in the Kinetic Analysis of Solid-State Reactions. *Thermochim. Acta* **2008**, *478* (1−2), 34−40.

(44) Valverde, J. M.; Sanchez-Jimenez, P. E.; Perez-Maqueda, L. Limestone Calcination Nearby Equilibrium: Kinetics, CaO Crystal Structure, Sintering and Reactivity. *J. Phys. Chem. C* **2015**, *119* (4), 1623−1641.

(45) Perejón, A.; Sánchez-Jiménez, P. E.; Criado, J. M.; Pérez-Maqueda, L. A. Magnesium Hydride for Energy Storage Applications: The Kinetics of Dehydrogenation under Different Working Conditions. *J. Alloys Compd.* **2016**, *681*, 571−579.

(46) Barin, I. *Thermochemical Data of Pure Substances*; VCH: Weinheim, 1989.

(47) Stanmore, B. R.; Gilot, P. Review—calcination and Carbonation of Limestone during Thermal Cycling for CO₂ Sequestration. *Fuel Process. Technol.* **2005**, *86* (16), 1707−1743.

(48) García-Labiano, F.; Abad, A.; de Diego, L. F.; Gayán, P.; Adánez, J. Calcination of Calcium-Based Sorbents at Pressure in a Broad Range of CO₂ Concentrations. *Chem. Eng. Sci.* **2002**, *57* (13), 2381−2393.

(49) Campbell, C. T.; Sellers, J. R. V. The Entropies of Adsorbed Molecules. *J. Am. Chem. Soc.* **2012**, *134* (43), 18109−18115.

(50) Negi, A. S.; Anand, S. C. *A Textbook of Physical Chemistry*; Wiley Eastern, 1985.

(51) Criado, J.; González, M.; Málek, J.; Ortega, A. The Effect of the CO₂ Pressure on the Thermal Decomposition Kinetics of Calcium Carbonate. *Thermochim. Acta* **1995**, *254* (121), 121−127.

(52) Khawam, A.; Flanagan, D. R. Solid-State Kinetic Models: Basics and Mathematical Fundamentals. *J. Phys. Chem. B* **2006**, *110* (35), 17315−17328.

(53) Brown, M. E. The Prout-Tompkins Rate Equation in Solid-State Kinetics. *Thermochim. Acta* **1997**, *300* (1−2), 93−106.

(54) Sánchez-Jiménez, P. E.; Perejón, A.; Pérez-Maqueda, L. A.; Criado, J. M. New Insights on the Kinetic Analysis of Isothermal Data: The Independence of the Activation Energy from the Assumed Kinetic Model. *Energy Fuels* **2015**, *29* (1), 392−397.

(55) Valverde, J. M.; Sanchez-Jimenez, P. E.; Perez-Maqueda, L. Ca-Looping for Postcombustion CO₂ Capture: A Comparative Analysis on the Performances of Dolomite and Limestone. *Appl. Energy* **2015**, *138*, 202−215.

(56) Wang, K.; Hu, X.; Zhao, P.; Yin, Z. Natural Dolomite Modified with Carbon Coating for Cyclic High-Temperature CO₂ Capture. *Appl. Energy* **2016**, *165*, 14−21.

(57) Sun, R.; Li, Y.; Liu, H.; Wu, S.; Lu, C. CO₂ Capture Performance of Calcium-Based Sorbent Doped with Manganese Salts during Calcium Looping Cycle. *Appl. Energy* **2012**, *89* (1), 368−373.

(58) Manovic, V.; Anthony, E. J. Thermal Activation of CaO-Based Sorbent and Self-Reactivation during CO₂ Capture Looping Cycles. *Environ. Sci. Technol.* **2008**, *42* (11), 4170−4174.

(59) Valverde, J. M.; Sanchez-jimenez, P. E.; Perejon, A.; Perez-maqueda, L. A. Role of Looping-Calcination Conditions on Self-Reactivation of Thermally Pretreated CO₂ Sorbents Based on CaO. *Energy Fuels* **2013**, *27*, 3373−3384.

(60) Valverde, J. M. *Relevant Influence of Limestone Crystallinity on CO₂ Capture in The Ca-Looping Technology at Realistic Calcination Conditions*; 2014.

(61) Manovic, V.; Anthony, E. J. Carbonation of CaO-Based Sorbents Enhanced by Steam Addition. *Ind. Eng. Chem. Res.* **2010**, *49* (19), 9105−9110.

(62) Alovisio, A.; Chacartegui, R.; Ortiz, C.; Valverde, J. M.; Verda, V. Optimizing the CSP-Calcium Looping Integration for Thermochemical Energy Storage. *Energy Convers. Manage.* **2017**, *136*, 85−98.

(63) Valverde, J. M. A Model on the CaO Multicyclic Conversion in the Ca-Looping Process. *Chem. Eng. J.* **2013**, *228*, 1195−1206.

(64) Obermeier, J.; Sakellariou, K. G.; Tsongidis, N. I.; Baciu, D.; Charalambopoulou, G.; Steriotis, T.; Müller, K.; Karagiannakis, G.; Konstandopoulos, A. G.; Stubos, A.; et al. Material Development and Assessment of an Energy Storage Concept Based on the CaO-Looping Process. *Sol. Energy* **2017**, *150*, 298−309.

(65) Valverde, J. M.; Sanchez-Jimenez, P. E.; Perez-Maqueda, L. Role of Precalcination and Regeneration Conditions on Postcombustion CO₂ Capture in the Ca-Looping Technology. *Appl. Energy* **2014**, *136*, 347−356.

(66) Alonso, M.; Rodríguez, N.; Grasa, G.; Abanades, J. C. Modelling of a Fluidized Bed Carbonator Reactor to Capture CO₂ from a Combustion Flue Gas. *Chem. Eng. Sci.* **2009**, *64* (5), 883−891.

(67) Abanades, J. C. The Maximum Capture Efficiency of CO₂ Using a Carbonation/calcination Cycle of CaO/CaCO3. *Chem. Eng. J.* **2002**, *90* (3), 303−306.

(68) Arias, B.; Abanades, J. C.; Grasa, G. S. An Analysis of the Effect of Carbonation Conditions on CaO Deactivation Curves. *Chem. Eng. J.* **2011**, *167* (1), 255−261.

(69) Mess, D.; Sarofim, A. F.; Longwell, J. P. Product Layer Diffusion during the Reaction of Calcium Oxide with Carbon Dioxide. *Energy Fuels* **1999**, *13* (5), 999−1005.

(70) Edwards, S. E. B.; Materić, V. Calcium Looping in Solar Power Generation Plants. *Sol. Energy* **2012**, *86* (9), 2494−2503.

(71) Fidaros, D. K.; Baxevanou, C. a.; Vlachos, N. S. A Parametric Study of a Solar Calcinator Using Computational Fluid Dynamics. *Energy Convers. Manage.* **2007**, *48* (11), 2784−2791.

(72) Meier, A.; Bonaldi, E.; Cella, G. M.; Lipinski, W.; Wuillemin, D. Solar Chemical Reactor Technology for Industrial Production of Lime. *Sol. Energy* **2006**, *80* (10), 1355−1362.

(73) Reich, L. Towards Solar Thermochemical Carbon Dioxide Capture via Calcium Oxide Looping: A Review. *Aerosol Air Qual. Res.* **2014**, *14* (2), 500−514.

(74) Koepf, E.; Alxneit, I.; Wieckert, C.; Meier, A. A Review of High Temperature Solar Driven Reactor Technology: 25years of Experience in Research and Development at the Paul Scherrer Institute. *Appl. Energy* **2017**, *188*, 620−651.

(75) Meier, A.; Gremaud, N.; Steinfeld, A. Economic Evaluation of the Industrial Solar Production of Lime. *Energy Convers. Manage.* **2005**, *46* (6), 905−926.

(76) Kvamsdal, H. M.; Romano, M. C.; van der Ham, L.; Bonalumi, D.; van Os, P.; Goetheer, E. Energetic Evaluation of a Power Plant Integrated with a Piperazine-Based CO₂ Capture Process. *Int. J. Greenhouse Gas Control* **2014**, *28*, 343−355.

(77) Romano, M. C. Modeling the Carbonator of a Ca-Looping Process for CO₂ Capture from Power Plant Flue Gas. *Chem. Eng. Sci.* **2012**, *69* (1), 257−269.

(78) MacKenzie, A.; Granatstein, D. L.; Anthony, E. J.; Abanades, J. C. Economics of CO₂ Capture Using the Calcium Cycle with a

Pressurized Fluidized Bed Combustor. *Energy Fuels* **2007**, *21* (2), 920−926.

(79) Abanades, J. C.; Grasa, G.; Alonso, M.; Rodriguez, N.; Anthony, E. J.; Romeo, L. M. Cost Structure of a Postcombustion CO_2 Capture System Using CaO. *Environ. Sci. Technol.* **2007**, *41* (15), 5523−5527.

(80) Romano, M. C.; Spinelli, M.; Campanari, S.; Consonni, S.; Cinti, G.; Marchi, M.; Borgarello, E. The Calcium Looping Process for Low CO_2 Emission Cement and Power. *Energy Procedia* **2013**, *37*, 7091−7099.

(81) Cormos, C.-C. Economic Evaluations of Coal-Based Combustion and Gasification Power Plants with Post-Combustion CO_2 Capture Using Calcium Looping Cycle. *Energy* **2014**, *78*, 665−673.